Anisotropic tunneling resistance in a phosphorene-based magnetic barrier

Feng Zhai, Wei Hu, and Junqiang Lu
Department of Physics, Zhejiang Normal University, Jinhua 321004, China
(Received 3 July 2017; revised manuscript received 20 September 2017; published 10 October 2017)

We investigate the ballistic tunneling transport properties of a monolayer of black phosphorus under a magnetic barrier. The conductance of the system depends strongly on the orientation of the magnetic barrier, which is suppressed maximally when the magnetic barrier is oriented along the armchair direction. The mechanism relies on the highly anisotropic energy dispersion of phosphorene and the magnetic-barrier-induced suppression of available phase space for transmission. The magnetoresistance is enhanced by the reduction of the band gap under the same effective mass components.

DOI: 10.1103/PhysRevB.96.165416

I. INTRODUCTION

The successful fabrication of graphene monolayer [1] has ignited a wave of research interest on two-dimensional (2D) materials. These materials consist of a single layer of one or several atoms and have various potential applications in nanoelectronics and nanophotonics. Phosphorene, a single layer of black phosphorus (BP), is a promising 2D material with a finite bulk band gap [2–4]. A BP film can be viewed as layers of phosphorus atoms stacked together by weak van der Waals forces. As the thickness of the BP film decreases from the bulk limit to a monolayer, the direct band gap is increasing continuously from 0.33 to 1.5–2 eV. The honeycomb network in phosphorene is strongly puckered due to the sp^3 hybridization. Accordingly, near the band edges the effective mass along the armchair direction differs greatly from that along the zigzag direction [5–8].

The presence of a considerable band gap and highly anisotropic band dispersion renders phosphorene distinctive from other 2D materials [9] such as monolayered graphene, BN, transition-metal dichalcogenides, silicene, and germanane. It has been reported experimentally that field-effect transistors based on phosphorene can possess an on/off ratio of 10^5 and a carrier mobility 10^3 cm^2/V s at room temperature [2,3]. The band gap of phosphorene and few-layer BP films can be tuned drastically by electric fields [10–14] due to the adsorption of potassium atoms or the application of gate voltages. The giant Stark effect can drive the material into a Dirac semimetal [13] with a linear dispersion in the armchair direction but quadratic dispersion in the zigzag direction. The unusual band anisotropy has been confirmed from the optical and transport measurements [2,15]. It has been utilized to design unconventional thermoelectric devices [16] and anomalous magneto-optical response [17]. For BP 2D electron systems under a uniform magnetic field, integer quantum Hall effect has been observed [18] and various magnetic quantization effects have been studied [19–23]. For a phosphorene nanoring under uniform magnetic fields, giant magnetoresistance (MR) has been predicted as a result of destructive interference phase caused by the Aharonov-Bohm effect [24]. The effect of inhomogeneous magnetic fields on the transport properties of phosphorene has not yet been explored so far.

In this work we investigate MR in a phosphorene-based magnetic barrier structure. The required inhomogeneous magnetic field has a finite spatial average. It can be generated by depositing ferromagnetic metals or superconducting materials above the phosphorene layer, the same as in semiconductor heterostructures [25–29]. This kind of magnetic barrier has been proposed to confine Dirac-Weyl quasiparticles [30] in graphene and to build a graphene-based valley filter [31]. For conduction electrons in 2D and 3D semiconductor heterostructures [32–34], the tunneling transparency and transport effects caused by such a magnetic barrier have been investigated in detail. For the considered system, one effect of the magnetic barrier is that the two isoenergy surfaces respectively in the ingoing and outgoing regions have a relative shift in the momentum space [30–34]. Due to the high anisotropy of the isoenergy surface in phosphorene, the number of allowed transmission channels depends strongly on the orientation of the magnetic barrier, leading to an anisotropic MR.

II. MODEL AND FORMULA

The system under consideration is a phosphorene 2D electron system in the (x,y) plane under the modulation of a local perpendicular magnetic field $\mathbf{B}(\mathbf{r})$, as depicted in the inset of Fig. 1(a). The x axis is along the armchair direction. The magnetic field varies along the ξ direction and is uniform along the perpendicular η direction, $B_z(\mathbf{r}) = B_z(\xi)$. Here the $+\xi$ axis is the transport direction and has an orientation angle α ($0 \leqslant \alpha \leqslant \pi/2$) relative to the x axis. It should be emphasized here that in our model the transport direction is always perpendicular to the orientation of the magnetic barrier. The Landau gauge is taken for the corresponding vector potential, $\mathbf{A}(\mathbf{r}) = A_\eta(\xi)\mathbf{e}_\eta$ with $A_\eta(\xi) = \int_{-\infty}^{\xi} B_z(\xi)d\xi$ and $A_\eta(-\infty) = 0$. The momentum operators $\hat{p}_x = -i\hbar\partial_x$ and $\hat{p}_y = -i\hbar\partial_y$ are linear combinations of $\hat{p}_\xi = -i\hbar\partial_\xi$ and $\hat{p}_\eta = -i\hbar\partial_\eta$. One has $\hat{p}_x = \hat{p}_\xi \cos\alpha - \hat{p}_\eta \sin\alpha$ and $\hat{p}_y = \hat{p}_\eta \cos\alpha + \hat{p}_\xi \sin\alpha$.

The motion of an electron in the system can be described by a two-band effective-mass model [6]

$$\hat{H} = \begin{pmatrix} \frac{\hat{\Pi}_x^2}{2m_{xc}} + \frac{\hat{\Pi}_y^2}{2m_{yc}} & \gamma\hat{\Pi}_x/\hbar \\ \gamma\hat{\Pi}_x/\hbar & -E_g - \frac{\hat{\Pi}_x^2}{2m_{xv}} - \frac{\hat{\Pi}_y^2}{2m_{yv}} \end{pmatrix}, \quad (1)$$

where the bottom of the conduction band is set as the energy zero, $\hat{\Pi}_{x,y} = \hat{p}_{x,y} + eA_{x,y}$, and E_g is the band gap. Without

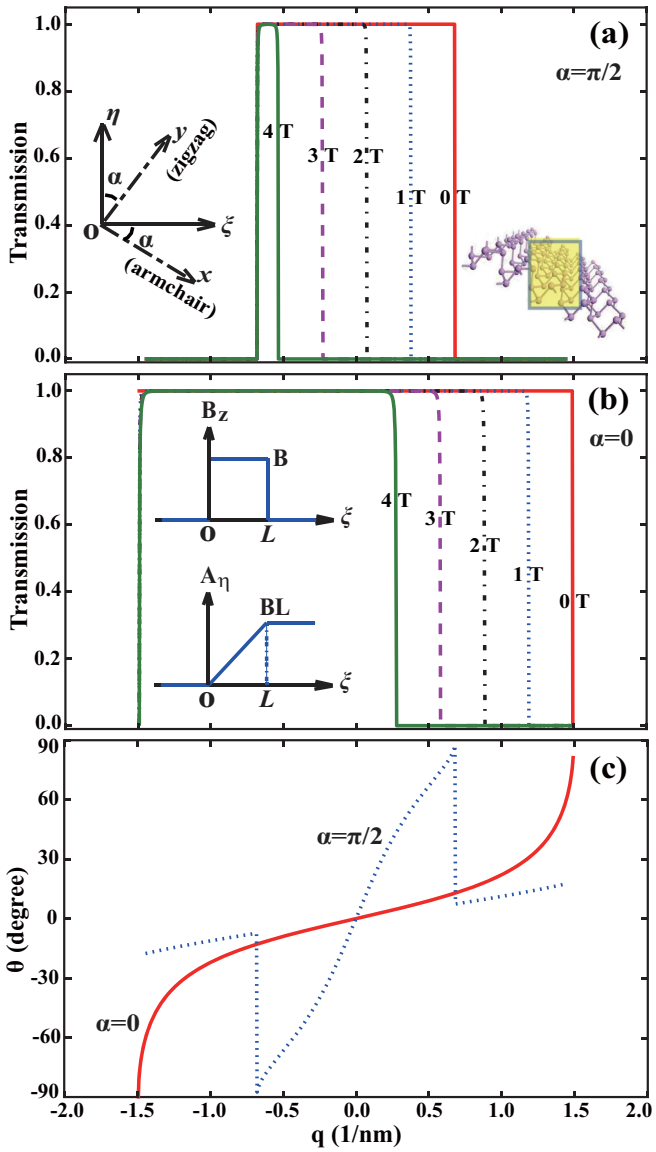

FIG. 1. Transmission as a function of the transverse wave vector q for electrons traversing the magnetic barrier with height $B = 0,1,2,3,4$ T. The transport is along the y (zigzag) direction in (a) and the x (armchair) direction in (b). The incident angle θ is plotted in (c) as a function of q for the armchair (solid line) and zigzag (dotted line) transport direction. Other parameters are $E_g = 1.52$ eV, $E = 0.1$ eV, and $L = 200$ nm. The inset of (a) depicts the considered phosphorene electron system under a rectangular magnetic barrier (the shadowed region). The profile of the local magnetic field B_z and its vector potential component A_η are shown in the inset of (b).

specification, E_g is taken as [6] 1.52 eV (the measured optical gap [3] is 1.45 eV). The parameters in the Hamiltonian are [6,19] the interband coupling $\gamma = -0.523\,05$ eV nm and the effective mass $(m_{xc},m_{xv},m_{yc},m_{yv}) = (0.793,0.848, 1.363,1.142)m_0$, where m_0 is the mass of a free electron in vacuum. Under the periodic boundary condition along the $O\eta$ axis, the transverse momentum $\hat{p}_\eta$ is conserved and takes the values $\hbar q$ with $q = 2\pi n/W$ $(n \in Z)$, where W is the size of the sample along the η direction. The velocity operator along the ξ and η directions, $\hat{v}_\xi = \frac{\partial \hat{H}}{\partial \hat{p}_\xi}$ and $\hat{v}_\eta = \frac{\partial \hat{H}}{\partial \hat{p}_\eta}$, read

$$\hat{v}_\xi = \begin{pmatrix} \frac{\hat{\Pi}_x \cos\alpha}{m_{xc}} + \frac{\hat{\Pi}_y \sin\alpha}{m_{yc}} & \frac{\gamma}{\hbar}\cos\alpha \\ \frac{\gamma}{\hbar}\cos\alpha & -\frac{\hat{\Pi}_x \cos\alpha}{m_{xv}} - \frac{\hat{\Pi}_y \sin\alpha}{m_{yv}} \end{pmatrix},$$

$$\hat{v}_\eta = \begin{pmatrix} \frac{\hat{\Pi}_y \cos\alpha}{m_{yc}} - \frac{\hat{\Pi}_x \sin\alpha}{m_{xc}} & -\frac{\gamma}{\hbar}\sin\alpha \\ -\frac{\gamma}{\hbar}\sin\alpha & \frac{\hat{\Pi}_x \sin\alpha}{m_{xv}} - \frac{\hat{\Pi}_y \cos\alpha}{m_{yv}} \end{pmatrix}. \quad (2)$$

For the electron with a given incident energy E and transverse wave vector q, the eigenwave function of Eq. (1) admits the form $\Psi(\mathbf{r}) = \exp(iq\eta)\psi(\xi)$. The longitudinal wave function $\psi(\xi)$ satisfies a one-dimensional Schrödinger equation $\hat{H}_q\psi(\xi) = E\psi(\xi)$, where $\hat{H}_q$ is obtained from Eq. (1) with the replacement $\hat{p}_\eta \to \hbar q$. In the ingoing/outgoing region the vector potential is constant and the dispersion relation of the electron is determined from

$$\left(E - \frac{\Pi_x^2}{2m_{xc}} - \frac{\Pi_y^2}{2m_{yc}}\right)\left(E' + \frac{\Pi_x^2}{2m_{xv}} + \frac{\Pi_y^2}{2m_{yv}}\right) = \left(\frac{\gamma\Pi_x}{\hbar}\right)^2, \quad (3)$$

where $\Pi_x = p_{\pm\infty}\cos\alpha - [q + eA_\eta(\pm\infty)]\sin\alpha$, $\Pi_y = p_{\pm\infty}\sin\alpha + [q + eA_\eta(\pm\infty)]\cos\alpha$, and $E' = E + E_g$. In the case that Eq. (3) has a real solution $p_{\pm\infty}$ in both the ingoing and outgoing regions, the electron has a finite probability $T(E,q)$ to transport through the magnetic barrier. In this situation there exists only one incident mode $\Psi_{in}(\mathbf{r}) = \exp(iq\eta + ip_{-\infty}\xi)\Phi$, where Φ is position independent; $p_{-\infty}$ is chosen to satisfy that Ψ_{in} has a positive group velocity along the transport direction, i.e., $v_\xi = \Psi_{in}^+\hat{v}_\xi\Psi_{in} > 0$. The incident angle θ relative to the transport direction is defined as $\theta = \arctan v_\eta/v_\xi$ with $v_\eta = \Psi_{in}^+\hat{v}_\eta\Psi_{in}$. The transmission probability $T(E,q)$ can be calculated numerically from $\hat{H}_q\psi(\xi) = E\psi(\xi)$ by means of the scattering matrix method [35,36], where the continuity of the wave function ψ and $\hat{v}_\xi\psi$ is used.

The ballistic conductance at zero temperature is given by the Landauer-Buttiker formula

$$G = \frac{2e^2}{2\pi\hbar}\sum_q T(E,q) = G_0\int_{-q_{\max}}^{q_{\max}} dq\, T(E,q), \quad (4)$$

where $G_0 = \frac{2e^2}{2\pi\hbar}\frac{W[nm]}{2\pi}$ is taken as the unit of the conductance when the wave vector q is in units of nm^{-1}, and $q_{\max} = \sqrt{2\max(m_{cx},m_{cy})E/\hbar}$ is an upper bound of q.

III. RESULTS AND DISCUSSIONS

We apply the theory formulated above to a square-well magnetic barrier [30,31] with height B and length L, i.e., $B_z(\mathbf{r}) = B\Theta(\xi)\Theta(L-\xi)$ in the $\xi O\eta$ coordinate system. Here $\Theta(x)$ is the Heaviside step function. The profile of the magnetic barrier and its vector potential component A_η are shown in the inset of Fig. 1(b). Note that the vector potential in the outgoing region differs from that in the ingoing region. This fact is required to demonstrate the operating principle of the proposed device which actually does not rely on the details of the barrier profile. For other shapes of the magnetic barrier, the wave-vector-filtering effect may lead to additional transmission features [29].

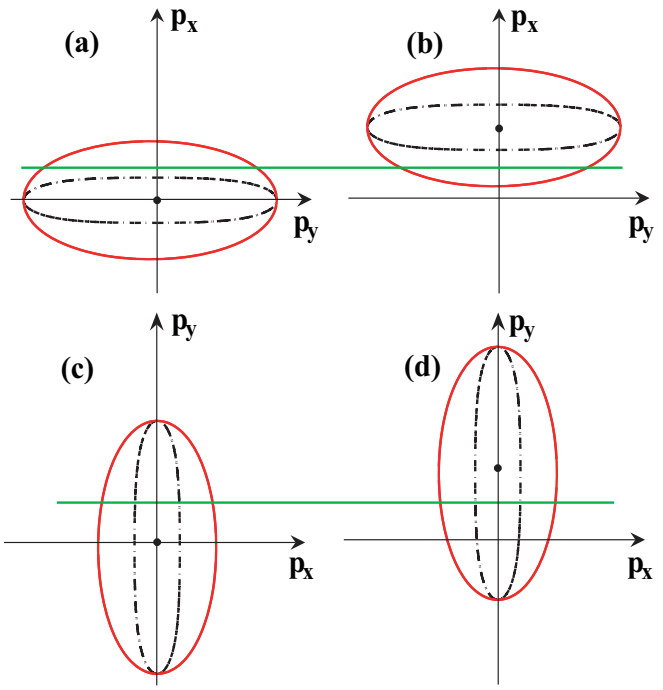

FIG. 2. Contour of constant energy in the ingoing (left panels) and outgoing (right panels) regions. In (a) and (b) the transport is along the y (zigzag) direction, while in (c) and (d) it is along the x (armchair) direction. The dot-dashed lines are for the anisotropic Dirac semimetal ($E_g = 0$). The horizontal line represents the conserved transverse momentum $\hbar q$.

For a typical Fermi energy $E = 0.1$ eV and length $L = 200$ nm, the transmission is plotted in Fig. 1 as a function of the transverse wave vector q for the considered system under different barrier heights $B = 0,1,2,3,4$ T. A common feature of all transmission curves is that the transmission is almost perfect in an interval of the wave vector q and vanishes outside that interval. As a result, the conductance in Eq. (4) is nearly proportional to the size of this transmission window. The transmission window of allowed transverse momentum shrinks as the height of the magnetic barrier increases. The shrinkage of the transmission window depends strongly on the orientation of the magnetic barrier. As the barrier height increases from 0 to 4 T, the size of the transmission window decreases drastically when the transport is along the zigzag direction [Fig. 1(a)]. It varies from 1.4 to 0.2 nm^{-1}. In the case that the transport is along the armchair direction [Fig. 1(b)], the magnetic barrier leads only to a moderate shrinkage of the transmission window. To compare with the transmission spectrum in Ref. [30] for Dirac particles in graphene under a rectangular magnetic barrier, in Appendix A we also plot the transmission as a function of the incident angle θ. A remarkable feature of the considered phosphorene system is that for the zigzag transport direction two different transverse wave vectors can correspond to the same incident angle, as shown in Fig. 1(c).

The transmission contrast between the armchair and zigzag transport directions can be understood from the relative position of the isoenergy surface in the ingoing and outgoing regions, which is shown in Fig. 2. The isoenergy surface is determined from Eq. (3). In the ingoing region (with $A_\eta \equiv 0$), it is an oval centered at the Γ point and has a highest point and a lowest point with transverse momentum $\pm p_L$. From Figs. 2(a) and 2(c), one can see that the value of p_L depends strongly on the transport direction due to the high anisotropy of the band dispersion. In the outgoing region with a finite $A_\eta \equiv BL$, the center of the isoenergy surface is shifted along the p_η axis with an amount eBL. The conservation of the transverse momentum determines the sector of allowed wave vector q for which propagating modes exist in both regions. One thus can estimate the size of the transmission window as $\max(0, 2p_L - eBL)$. The magnetic barrier can close the transmission window more easily for a smaller p_L, as shown in Figs. 2(b) and 2(d).

It should be pointed out that for spinful electrons in cubic semiconductors, the character of barrier tunneling depends also on the barrier orientation [37–40]. In this case the Dresselhaus spin-orbit interaction depends sensitively on the crystallographic direction of the barrier. Accordingly, the barrier transparency depends on the barrier orientation relative to the crystallographic axes and the direction of the mean spin of tunneling electrons. For semiconductor heterostructures with double quantum wells separated by a tunneling barrier [41,42], the effect of in-plane magnetic fields on the energy spectrum and spin-related transport has also been widely studied theoretically and experimentally.

The transmission features demonstrated above can be reflected directly from the measurable conductance spectrum, which is shown in Fig. 3. It is evident that the onset of the conductance as a function of the Fermi energy depends on both the height and the orientation of the magnetic barrier. One can estimate the transition energy as follows. For a large band gap $E_g = 1.52$ eV, the interband coupling in Eq. (1) can be treated perturbatively and a decoupled Hamiltonian is obtained [19]:

$$\hat{H} \approx \begin{pmatrix} \frac{\hat{\Pi}_x^2}{2m'_{xc}} + \frac{\hat{\Pi}_y^2}{2m_{yc}} & 0 \\ 0 & -E_g - \frac{\hat{\Pi}_x^2}{2m'_{xv}} - \frac{\hat{\Pi}_y^2}{2m_{yv}} \end{pmatrix}, \qquad (5)$$

where $m'_{xc} = 0.167m_0$ and $m'_{xv} = 0.184m_0$ are calculated from $1/m'_{xc/v} = 1/m_{xc/v} + 2(\gamma/\hbar)^2/E_g$. From the decoupled Hamiltonian, one finds that $p_L = \sqrt{2m_{yc}E} = \sqrt{1.696m_0E}$ for the transport x (armchair) direction and $p_L = \sqrt{2m'_{xc}E} = \sqrt{0.334m_0E}$ for the transport y (zigzag) direction. The transition energy E_0 satisfies $p_L(E_0) = eBL/2$. Under the same barrier height B, the zero conductance region in the conductance spectrum for the zigzag transport direction is much broader than that for the armchair transport direction. Although the numerical results are presented only for the Fermi energy near the conduction band ($E > 0$), similar analysis can be made for the Fermi energy near the valence band ($E < -E_g$). For $E < -E_g$ there exists a more remarkable contrast between the conductance for the armchair transport direction and that for the zigzag transport direction.

For other orientation angles of the transport direction, the transition energy E_0 in the conductance spectrum is in between the value for the armchair direction and the value for the zigzag direction. In Fig. 4, the conductance is plotted as a function of the orientation angle α under the Fermi energy $E = 0.1$ eV and several barrier heights. It can be seen

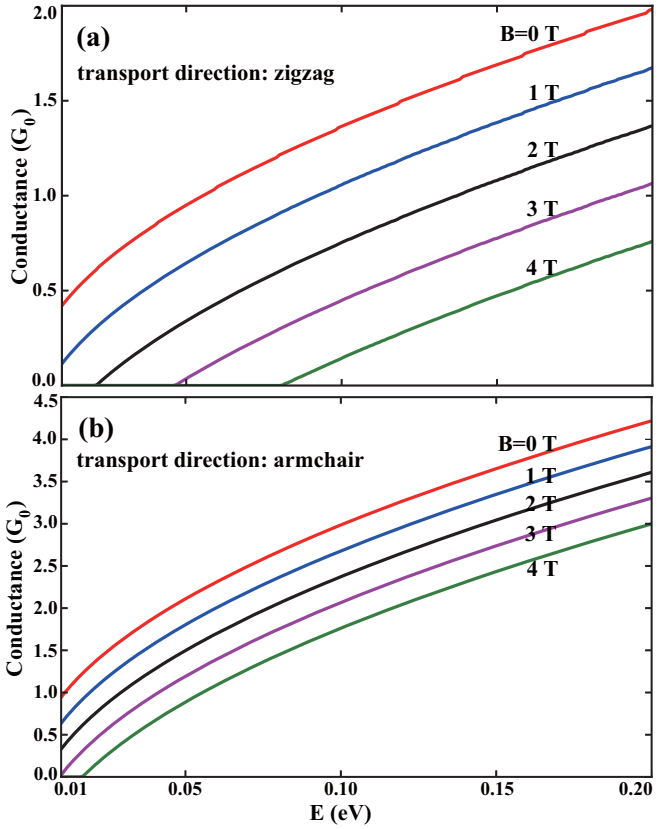

FIG. 3. Conductance as a function of the Fermi energy for the phosphorene-based magnetic barrier under different barrier heights $B = 0,1,2,3,4$ T. (a) The transport is along the zigzag direction. (b) The transport is along the armchair direction. $L = 200$ nm.

that for all curves the conductance decreases monotonously from the orientation angle $\alpha = 0$ to $\alpha = 90^\circ$. To examine the conductance anisotropy, it is sufficient to calculate the conductance under the orientation angles $\alpha = 0$ and $\alpha = 90^\circ$.

From the transmission features one can estimate the conductance for $E > E_0$ as

$$G \approx G_0(2p_L - eBL). \tag{6}$$

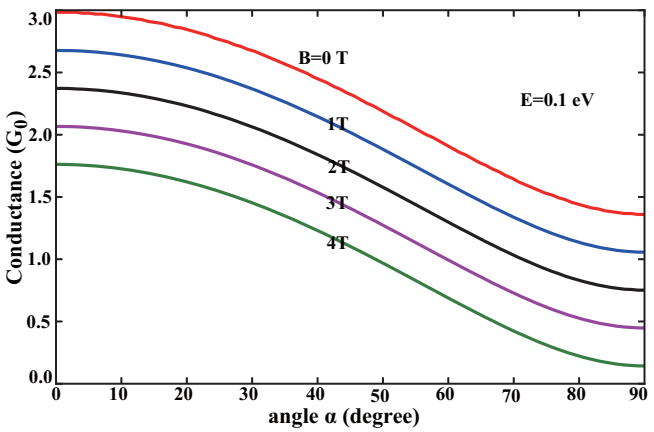

FIG. 4. Conductance as a function of the orientation angle α of the transport direction under different barrier heights $B = 0,1,2,3,4$ T. The Fermi energy is fixed at $E = 0.1$ eV.

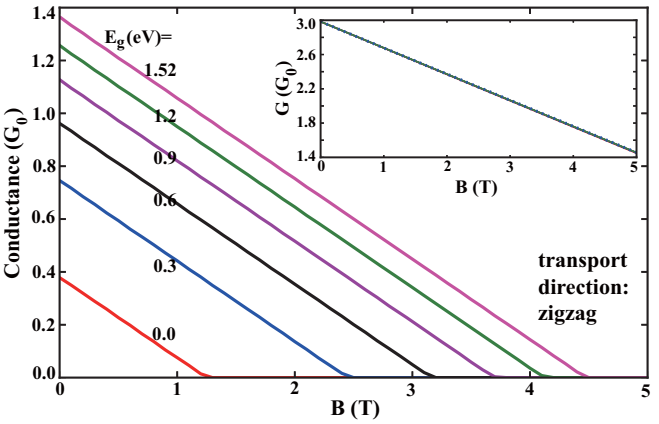

FIG. 5. Conductance as a function of the height of the magnetic barrier B under different band gaps $E_g = 0.0,0.3,0.6,0.9,1.2,1.52$ eV. The transport is along the zigzag direction. The inset shows the results for the transport along the armchair direction. The Fermi energy is fixed at $E = 0.1$ eV.

The estimated conductance decreases linearly with the barrier height B, which agrees well with the accurate calculations (not shown here). The conductance is suppressed completely for $B > B_c \approx 2p_L/(eL)$. The critical magnetic field $B_c \leqslant 4.5$ T is moderate for the transport along the zigzag direction and Fermi energy $E \leqslant 0.1$ eV. A large barrier height B (>5 T) is needed to pinch off the transport along the armchair direction even for a small Fermi energy $E = 0.05$ eV. One can reduce the critical magnetic field B_c by increasing the width L of the magnetic barrier. For a Fermi energy E, the MR due to the magnetic barrier with height B is defined as $R_M(E,B) = [G(E,0) - G(E,B)]/G(E,0)$. For B higher than the critical magnetic field B_c, the ballistic conductance $G(E,B)$ can result only from the edge channels. In a wide phosphorene sample, the number of edge channels is a negligibly small part of the whole transmission channels. In this case $G(E,B) \ll G(E,0)$ and a giant MR is expected.

Finally, we discuss the effect of band gap on the MR. A theoretical calculation indicates [10] that a perpendicular electric field F can enlarge the band gap of phosphorene. The effective mass components change slightly under $F < 1$ V/Å. The tunability of band gap in few-layered BP films has been demonstrated [11] where the conduction and valence band almost unchange their structures. It is thus feasible to keep other material parameters in Eq. (1) unchanged when we examine the effect of band gap. Figure 5 shows the conductance as a function of barrier height under several values of band gap E_g. The Fermi energy is fixed at $E = 0.1$ eV above the bottom of the conduction band. For small band gaps, the conductance also varies linearly with the barrier height B according to Eq. (6). However, for a small E_g the critical magnetic field B_c cannot be calculated from the decoupled Hamiltonian, Eq. (5). For the transport along the zigzag direction, the critical magnetic field B_c decreases remarkably with the decreasing of band gap. As the material is tuned from a moderate-gap semiconductor ($E_g = 1.52$ eV) to a Dirac semimetal ($E_g = 0$), B_c shifts from 4.5 to 1.3 T. This indicates that under the same anisotropic effective-mass parameters and the same magnetic barrier, the Dirac semimetal has a more

pronounced MR than a semiconductor. The reason can be also found from the isoenergy surfaces for both materials shown in Fig. 2. From the inset of Fig. 5, one can see that for the transport along the armchair direction the MR has almost no dependence on the band gap. The MR anisotropy is more remarkable for the Dirac semimetal when the effective mass components are unchanged. For few-layered BP film with Fermi energy in between the bottoms of the first and the second conduction subbands, a similar calculation shown in Appendix B results in the same conclusion.

IV. CONCLUSIONS

In summary, we have investigated the ballistic transport properties of a phosphorene two-dimensional electron gas under a magnetic barrier. The average magnetic field of the magnetic barrier is finite. Such a magnetic barrier causes a relative shift in the momentum space between the isoenergy surfaces in the ingoing and outgoing regions. This fact together with the highly anisotropic energy dispersion of phosphorene leads to transport-direction-dependent suppression of available phase space for transmission. The conductance of the system depends strongly on the orientation of the magnetic barrier, which is suppressed maximally when the magnetic barrier is in parallel with the armchair direction. Giant magnetoresistance appears when all of bulk transmission channels are fully blocked by the magnetic barrier. Under the same effective mass components, the magnetoresistance anisotropy is enhanced by the reduction of the band gap.

ACKNOWLEDGMENT

This work was supported by the National Natural Science Foundation of China (Grant No. 11774314).

APPENDIX A: INCIDENT-ANGLE DEPENDENCE OF THE TRANSMISSION

In Fig. 6 we replot the transmission shown in Fig. 1 as a function of the incident angle θ. For the armchair (zigzag) transport direction, the transmission decreases gradually (abruptly) as the incident angle tends to -90°, while the transmission window of allowed incident angle shrinks moderately (greatly) as the height of the magnetic barrier increases from 0 to 4 T. For the zigzag transport direction, an incident angle may correspond to two different transverse wave vectors q_1 and q_2. However, the transmission under one of q_1 and q_2 is forbidden and is not shown in Fig. 6(a).

APPENDIX B: FEW-LAYERED BLACK PHOSPHORUS FILMS UNDER A MAGNETIC BARRIER

For few-layered BP films under a rectangular magnetic barrier, we can calculate the transmission and conductance by means of the same procedure. We take a hard wall boundary condition in the normal direction (the z axis). The Hamiltonian for the first subband of an N-layered BP film [7,17] has the same form as Eq. (1), but with the parameters $(m_{xc},m_{xv},m_{yc},m_{yv}) = (0.151,0.122,1.062,0.708)m_0$ and $\gamma = \hbar v_f$ with $v_f = 3.5 \times 10^5$ m/s. We consider the BP film with $N = 4$, which has a zero-field band gap $E_g = E_g^1/N^{0.73} + E_g^\infty = 1.03$ eV with $E_g^1 = 2.0$ eV and $E_g^\infty = 0.3$ eV. The band gap E_g can be reduced by a normally applied electric field [11,14]. In Fig. 7, the conductance is plotted as a function of barrier height under several values of band gap E_g. The bottom of the lowest conduction subband is set as energy zero. The Fermi energy is fixed at $E = 0.1$ eV, which is well below the bottom of the second conduction subband (located at

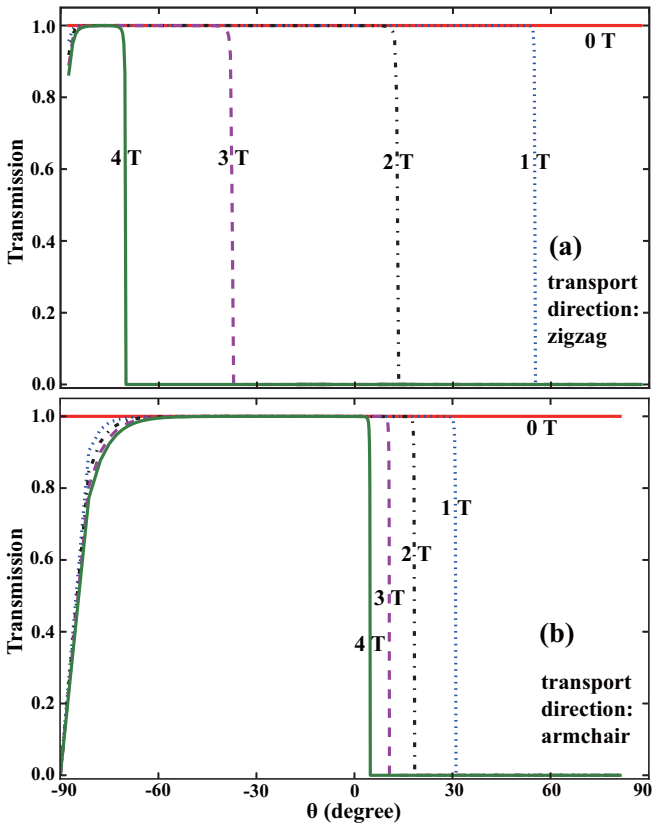

FIG. 6. Transmission as a function of the incident angle θ for electrons traversing the magnetic barrier with different heights $B = 0,1,2,3,4$ T. The transport is along the y (zigzag) direction in (a) and the x (armchair) direction in (b). The parameters are the same as in Fig. 1.

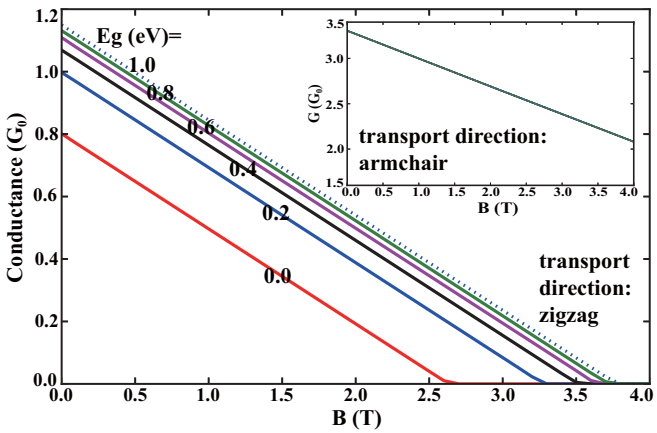

FIG. 7. The same as Fig. 5 but for a four-layered BP film with band gap $E_g = 0,0.2,0.4,0.6,0.8,1.0$ eV.

0.966 eV). In comparison with the results for the monolayered phosphorene (Fig. 5), here the pinch-off magnetic field B_c for the zigzag transport direction decreases more slowly with the reduction of the band gap.

[1] A. H. C. Neto, F. Guinea, N. M. R. Peres, K. S. Novoselov, and A. K. Geim, Rev. Mod. Phys. **81**, 109 (2009).

[2] L. Li, Y. Yu, G. J. Ye, Q. Ge, X. Ou, H. Wu, D. Feng, X. H. Chen, and Y. Zhang, Nat. Nanotechnol. **9**, 372 (2014).

[3] H. Liu, A. T. Neal, Z. Zhu, Z. Luo, X. Xu, D. Tomanek, and P. D. Ye, ACS Nano **8**, 4033 (2014).

[4] J. Qiao, X. Kong, Z.-X. Hu, F. Yang, and W. Ji, Nat. Commun. **5**, 4475 (2014).

[5] A. S. Rodin, A. Carvalho, and A. H. Castro Neto, Phys. Rev. Lett. **112**, 176801 (2014).

[6] M. Ezawa, New J. Phys. **16**, 115004 (2014).

[7] V. Tran, R. Soklaski, Y. Liang, and L. Yang, Phys. Rev. B **89**, 235319 (2014).

[8] R. Fei and L. Yang, Nano Lett. **14**, 2884 (2014).

[9] G. R. Bhimanapati *et al.*, ACS Nano **9**, 11509 (2015).

[10] M. Yang, H. J. Duan, and R.-Q. Wang, Phys. Scr. **91**, 105801 (2016).

[11] Q. Liu, X. Zhang, L. B. Abdalla, A. Fazzio, and A. Zunger, Nano Lett. **15**, 1222 (2015).

[12] K. Dolui and S. Y. Quek, Sci. Rep. **5**, 11699 (2015).

[13] J. Kim, S. S. Baik, S. H. Ryu, Y. Sohn, S. Park, B.-G. Park, J. Denlinger, Y. Yi, H. J. Choi, and K. S. Kim, Science **349**, 723 (2015).

[14] B. C. Deng, V. Tran, Y. J. Xie, H. Jiang, C. Li, Q. S. Guo, X. M. Wang, H. Tian, S. J. Koester, H. Wang, J. J. Cha, Q. F. Xia, L. Yang, and F. N. Xia, Nat. Commun. **8**, 14474 (2017).

[15] F. Xia, H. Wang, and Y. Jia, Nat. Commun. **5**, 4458 (2014).

[16] X. Ling, H. Wang, S. Huang, F. Xia, and M. S. Dresselhaus, Proc. Natl. Acad. Sci. USA **112**, 4523 (2015).

[17] X. Y. Zhou, W. K. Lou, F. Zhai, and K. Chang, Phys. Rev. B **92**, 165405 (2015).

[18] L. Li, F. Yang, G. J. Ye, Z. Zhang, Z. Zhu, W. Lou, X. Zhou, L. Li, K. Watanabe, T. Taniguchi, K. Chang, Y. Wang, X. H. Chen, and Y. Zhang, Nat. Nanotechnol. **11**, 593 (2016).

[19] X. Y. Zhou, R. Zhang, J. P. Sun, Y. L. Zou, D. Zhang, W. K. Lou, F. Cheng, G. H. Zhou, F. Zhai, and K. Chang, Sci. Rep. **5**, 12295 (2015).

[20] J. M. Pereira, Jr. and M. I. Katsnelson, Phys. Rev. B **92**, 075437 (2015).

[21] Z. T. Jiang, Z. T. Lv, and X. D. Zhang, Phys. Rev. B **94**, 115118 (2016).

[22] S. Yuan, E. van Veen, M. I. Katsnelson, and R. Roldan, Phys. Rev. B **93**, 245433 (2016).

[23] J. Y. Wu, S. C. Chen, G. Gumbs, and M. F. Lin, Phys. Rev. B **95**, 115411 (2017).

[24] R. Zhang, Z. H. Wu, X. J. Li, and K. Chang, Phys. Rev. B. **95**, 125418 (2017).

[25] A. Nogaret, S. J. Bending, and M. Henini, Phys. Rev. Lett. **84**, 2231 (2000).

[26] A. Nogaret, D. N. Lawton, D. K. Maude, J. C. Portal, and M. Henini, Phys. Rev. B **67**, 165317 (2003).

[27] J. Hong, S. Joo, T.-S. Kim, K. Rhie, K. H. Kim, S. U. Kim, B. C. Lee, and K.-H. Shinc, Appl. Phys. Lett. **90**, 023510 (2007).

[28] A. Tarasov, S. Hugger, H. Y. Xu, M. Cerchez, T. Heinzel, I. V. Zozoulenko, U. Gasser-Szerer, D. Reuter, and A. D. Wieck, Phys. Rev. Lett. **104**, 186801 (2010).

[29] For a review, see S. J. Lee, S. Souma, G. Ihm, and K. J. Chang, Phys. Rep. **394**, 1 (2004).

[30] A. De Martino, L. Dell'Anna, and R. Egger, Phys. Rev. Lett. **98**, 066802 (2007).

[31] F. Zhai and K. Chang, Phys. Rev. B **85**, 155415 (2012).

[32] P. Gueret, A. Baratoff, and E. Marclay, Europhys. Lett. **3**, 367 (1987).

[33] C. Heide, Phys. Rev. B **60**, 2571 (1999).

[34] P. S. Alekseev, JETP Lett. **92**, 788 (2010).

[35] H. Xu, Phys. Rev. B **50**, 8469 (1994).

[36] F. Zhai and J. Q. Lu, Phys. Rev. B **94**, 165426 (2016).

[37] V. I. Perel, S. A. Tarasenko, I. N. Yassievich, S. D. Ganichev, V. V. Bel'kov, and W. Prettl, Phys. Rev. B **67**, 201304 (2003).

[38] S. A. Tarasenko, V. I. Perel, and I. N. Yassievich, Phys. Rev. Lett. **93**, 056601 (2004).

[39] P. S. Alekseev, M. M. Glazov, and S. A. Tarasenko, Phys. Rev. B **89**, 155306 (2014).

[40] J. Moser, A. Matos-Abiague, D. Schuh, W. Wegscheider, J. Fabian, and D. Weiss, Phys. Rev. Lett. **99**, 056601 (2007).

[41] P. S. Alekseev, M. V. Yakunin, and I. N. Yassievich, Semiconductors **41**, 1092 (2007).

[42] M. V. Yakunin, G. A. Al'shanskii, Yu. G. Arapov, V. N. Neverov, G. I. Kharus, N. G. Shelushinina, B. N. Zvonkov, E. A. Uskova, A. de Visser, and L. Ponomarenko, Semiconductors **39**, 107 (2005).